Clim. Past, 12, 787–798, 2016
www.clim-past.net/12/787/2016/
doi:10.5194/cp-12-787-2016

Climate of the Past
Open Access
EGU

Terrigenous material supply to the Peruvian central continental shelf (Pisco, 14° S) during the last 1000 years: paleoclimatic implications

Francisco Javier Briceño-Zuluaga[1,2], Abdelfettah Sifeddine[1,2,3], Sandrine Caquineau[2,3], Jorge Cardich[1,2], Renato Salvatteci[5], Dimitri Gutierrez[2,4], Luc Ortlieb[2,3], Federico Velazco[2,4], Hugues Boucher[2,3], and Carine Machado[1,2]

[1]Departamento de Geoquímica, Universidade Federal Fluminense – UFF, Niterói, RJ, Brazil
[2]LMI PALEOTRACES (IRD-France, UPMC-France, UA-Chile, UFF-Brazil, UPCH-Peru), Brazil
[3]IRD-Sorbonne Universités (UPMC, CNRS-MNHN), LOCEAN, IRD France-Nord, Bondy, France
[4]Instituto del Mar del Peru IMARPE. Esquina Gamarra y General Valle s/n, Callao 22000, Peru
[5]Institute of Geoscience, Kiel University, Kiel, Germany

Correspondence to: Francisco Javier Briceño-Zuluaga (franciscojavier@id.uff.br)

Received: 16 June 2015 – Published in Clim. Past Discuss.: 17 July 2015
Revised: 13 February 2016 – Accepted: 15 March 2016 – Published: 31 March 2016

Abstract. In the eastern Pacific, lithogenic input to the ocean responds to variations in the atmospheric and oceanic system and their teleconnections over different timescales. Atmospheric (e.g., wind fields), hydrological (e.g., fresh water plumes) and oceanic (e.g., currents) conditions determine the transport mode and the amount of lithogenic material transported from the continent to the continental shelf. Here, we present the grain size distribution of a composite record of two laminated sediment cores retrieved from the Peruvian continental shelf that record the last ∼1000 years at a sub-decadal to centennial time-series resolution. We propose novel grain size indicators of wind intensity and fluvain ability modulated by sub-decadal to centennial changes in climatic conditions. Four grain size modes were identified. Two are linked to aeolian inputs (M3: ∼54; M4: ∼91 µm on average), the third is interpreted as a marker of sediment discharge (M2: ∼10 µm on average), and the last is without an associated origin (M1: ∼3 µm). The coarsest components (M3 and M4) dominated during the Medieval Climate Anomaly (MCA) and the Current Warm Period (CWP) periods, suggesting that aeolian transport increased as a consequence of surface wind stress intensification. In contrast, M2 displays an opposite behavior, exhibiting an increase in

toemorsehumide(codiatiose)253(associ)1(atede)253(withe)252(Ele)253(Niño-n)]TJT*[likt(codiatios.e)286(Comparisone)286(withe)286(o(h
vebyn intracatiosebetweanmeridtioial(displ)1(cementl)-72((of] TJ0 -11.955 TD[(hce)1942Iintrtropicale)195(Conr)40ve)15erguence(IT
(SPSH)linkkfatl

he Pisco region (∼ 14–15° S) hosts one of the most intense
oastal upwelling cells off Peru due to the magnitude and per-

terannual variations in the domain of the strongest winds. The Pisco region is also home to local dust storms called *Paracas*, which transport dust material to the continental shelf as a response to seasonal erosion and transport events in the Ica Desert (∼ 15° S). This process reflects atmospheric stability conditions and coastal sea surface temperature connections (Gay, 2005). In contrast, sediment fluvial discharge is more important on the northern coast of Peru, where there are large rivers, and it decreases southward, where arid conditions are dominant (Garreaud and Falvey, 2009; Scheidegger and Krissek, 1982). This discharged material is redistributed southward by coastal currents along the continental shelf (Montes et al., 2010; Smith, 1983). In addition, small rivers exist in our study area, such as the Pisco River, which can increase their flow during strong El Niño events (Bekaddour et al., 2014). It has also been demonstrated that, during El Niño events and coincident positive PDO, there is an increase in precipitation along northern Peru and, consequently, higher river discharge, mainly from the large rivers (e.g., the Santa River), whereas an opposite behavior is observed during La Niña events and the negative phase of PDO (Bekaddour et al., 2014; Böning and Brumsack, 2004; Lavado Casimiro et al., 2012; Ortlieb, 2000; Rein, 2005, 2007; Scheidegger and Krissek, 1982; Sears, 1954).

Grain size distributions in marine sediments may indicate different sources and/or depositional processes that can be expressed as polymodal distributions (e.g., Pichevin et al., 2005; Saukel et al., 2011; Stuut and Lamy, 2004; Stuut et al., 2002, 2007; Sun et al., 2002; Weltje and Prins, 2003, 2007). The polymodal distribution makes the classification of grain size composition an essential step in identifying the different sedimentary processes and the past environmental conditions behind them (e.g., climate, atmosphere and ocean circulation) (Bloemsma et al., 2012; Flores-Aqueveque et al., 2012, 2015; Pichevin et al., 2005; Ratmeyer et al., 1999; Saukel et al., 2011; Stuut et al., 2005, 2007; Sun et al., 2002). The grain size distributions of lithogenic materials in marine sediments can thus be used to infer relative wind strengths and aridity on the assumption that more vigorous atmospheric circulation will transport coarser particles to a greater distance and that the relative abundance of fluvial particles reflects precipitation patterns (e.g., Hesse and McTainsh, 1999; Parkin and Shackleton, 1973; Pichevin et al., 2005; Stuut and Lamy, 2004; Stuut et al., 2002).

A significant number of studies have described the climatic, hydrologic and oceanographic changes during the last 1000 years on the Peruvian continental shelf (Ehlert et al., 2015; Gutiérrez et al., 2011; Salvatteci et al., 2014b; Sifeddine et al., 2008). Evidence of changes in the Humboldt Current circulation system and in the precipitation pattern has been reported. Salvatteci et al. (2014b) show that the Medieval Climatic Anomaly (MCA) exhibits two distinct patterns of Peruvian upwelling characterized by weak/intense marine productivity and sub-surface oxygenation, respectively, as a response to the intensity of South Pacific Subtropical High (SPSH) linked to the Walker circulation. During the Little Ice Age (LIA), an increased sediment discharge over the Pisco continental shelf was described, as well as a stronger oxygenation and lower productivity (Gutiérrez et al., 2009; Salvatteci et al., 2014b; Sifeddine et al., 2008). In addition, during the Current Warm Period (CWP), the Peruvian Upwelling Ecosystem exhibited (1) an intense oxygen minimum zone (OMZ) and an increase in marine productivity, (2) a significant sea surface temperature cooling (∼0.3–0.4 °C decade^{-1}), and (3) an increase in terrigenous material input (Gutiérrez et al., 2011).

Here we present new data regarding the effective mode of transport of mineral fractions to the Pisco shelf during the last millennium, confirming previous work and bringing new knowledge about the climatic mechanism behind Humboldt circulation and atmospheric changes, especially during the MCA. Our results identify wind intensification during the second part of the MCA and CWP, in contrast to a decrease in the wind intensity during the LIA and the first part of the MCA synchronous with fluvial discharge increases. Comparisons with other paleoclimate records indicate that the ITCZ displacement, the SPSH and the Walker circulation were the main drivers for the hydroclimate changes along the coastal Peruvian shelf during the last millennium.

2 Sedimentary settings

Reinhardt et al. (2002), Suess et al. (1987) and Gutiérrez et al. (2006) described the sedimentary facies in the Peruvian shelf and the role of currents in the erosion process as well as the redistribution and favorable hemipelagic sedimentation of material over the continental shelf. These studies showed that high-resolution sediment records are present in specific localities of the Peruvian continental margin. Suess et al. (1987) described the two sedimentary characteristic facies between 6 and 10° S and between 11 and 16° S. The first one, 6–10° S (Salaverry Basin), is characterized by the absence of hemipelagic sediment accumulation, because in this zone the southward poleward undercurrent is strong. The second one, Lima Basin (11–16° S), is characterized by a lens-shaped depositional center of organic-rich mud facies favored by oceanographic dynamics from the position and low velocity of the southward poleward current on the continental shelf (Reinhardt et al., 2002; Suess et al., 1987). High-resolution sediment echo sounder profiles further characterize the mud lens nature and complement the continental shelf information (Salvatteci et al., 2014a). These upper mud lenses are characterized by fine grain size, a diatomaceous, hemiplegic mud with high organic carbon, and the absence of erosive and bioturbation processes.

The Pisco continental shelf sediments are a composite of laminated structures characterized by an array of more or less dense sections of dark and light millimetric laminae (Brodie and Kemp, 1994; Salvatteci et al., 2014a; Sifeddine et al.,

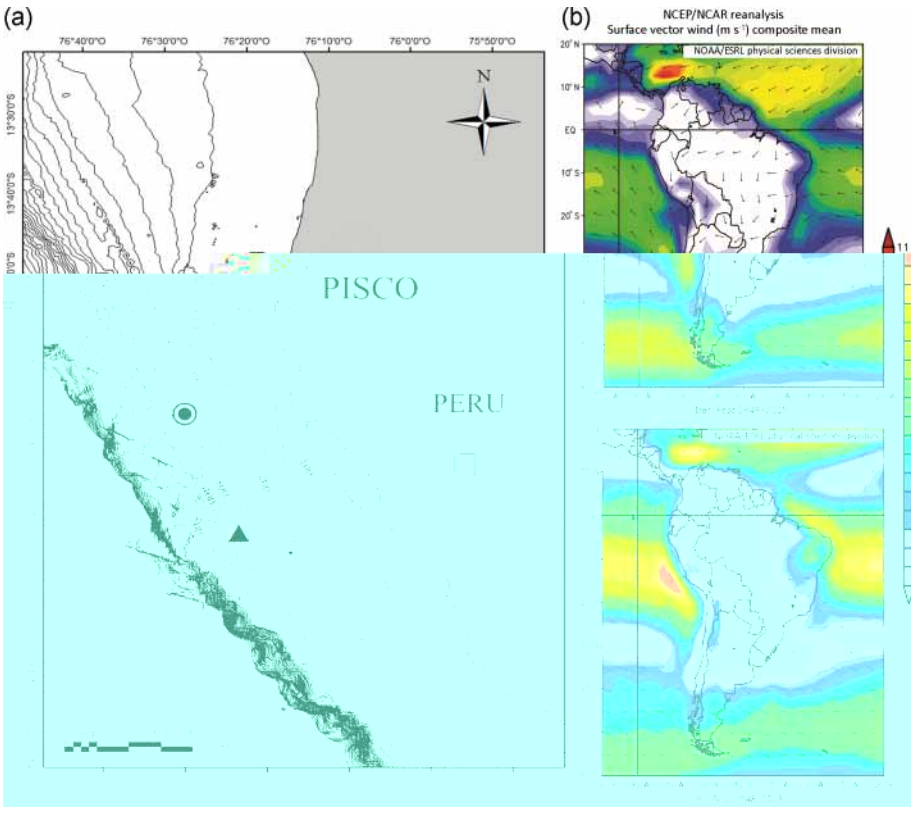

Figure 1. **(a)** Location of the sampling of the sediment cores B040506 (black circle) and G10-GC-01 (black triangle) in the central Peru continental margin. Bathymetric contour lines are in 25 m intervals from 100 to 500 m depth. **(b)** Mean surface vector wind velocity ($m\,s^{-1}$) composite mean for summer (up) and winter (down) between 1948 and 2015 for South America. NCEP/NCAR Reanalysis data.

2008). The laminae structure and composition result from a complex interplay of factors including the terrigenous material input (both aeolian and fluvial), the upwelling productivity, and associated particle export to the seafloor (Brodie and Kemp, 1994; Salvatteci et al., 2014a). The anoxic conditions favored by an intense OMZ (Gutiérrez et al., 2006) and weak current activity in some areas (Reinhardt et al., 2002; Suess et al., 1987) favor the preservation of paleoenvironmental signals and consequently a successful recording of the environmental and climate variability.

Along the Peruvian coast, lithogenic fluvial material is supplied by a series of large rivers that are more significant to the north of the study area (Lavado Casimiro et al., 2012; McPhillips et al., 2013; Morera et al., 2011; Rein, 2005; Scheidegger and Krissek, 1982; Unkel et al., 2007). In fact, Smith (1983) concluded that sedimentary material can be transported for long distances in an opposite direction of prevailing winds and surface currents in upwelling zones. In fact, the coastal circulation off Peru is dominated by the poleward Peru–Chile undercurrent (PCUC), which flows over the outer continental shelf and upper continental slope, whereas the equatorward Peru coastal current is limited to a few dozens of meters in the surface layer (Chaigneau et al., 2013). On the other hand, several works have shown that precipitation, fluvial input discharge (Bekaddour et al., 2014; Bendix et al., 2002; Lavado-Casimiro and Espinoza, 2014), and the PCUC increase during the El Niño events (Hill et al., 1998; Strub et al., 1998; Suess et al., 1987). These observations suggest a potential for the fluvial particles to spread over the continental margin under wet paleoclimatic conditions (e.g., El Niño or El Niño-like). Lithogenic material in the study area might also originate from wind-driven dust storms or *vientos Paracas*, which are more frequent and intense during austral winters (Escobar Baccaro, 1993; Gay, 2005; Haney and Grolier, 1991) and by the saltation and suspension mechanisms with which this material reaches the continental shelf.

3 Materials and methods

3.1 Stacked record

The B040506 (hereafter "B06"; 14°07.90′ S, 76°30.10′ W; 299 m water depth) and the G10-GC-01 (hereafter "G10"; 14°22.96′ S, 076°23.89′ W; 313 m water depth) sediment cores were retrieved from the central Peruvian continental shelf in 2004 during the Paleo2 cruise onboard the Peruvian vessel *José Olaya Balandra* (IMARPE) and in 2007

during the Galathea-3 cruise, respectively (Fig. 1a). We compared the age models and performed a laminae cross-correlation between the two cores in order to develop a continuous record for the last millennium (Salvatteci et al., 2014a) (Fig. S1 in the Supplement). The choice of these two cores was based on previous detailed stratigraphic investigations and available complementary multi-proxy reconstructions (Gutiérrez et al., 2006, 2009; Salvatteci et al., 2012, 2014a, b; Sifeddine et al., 2008). The box core B06 (0.75 m length) is a laminated core with a visible slump at ∼ 52 cm and three thick homogeneous deposits (1.5 to 5.0 cm thick) identified in the SCOPIX images. These intervals were not considered in our study (Fig. S1). The presence of filaments of the giant sulfur bacteria *Thioploca* spp. in the top of core B06 confirms the successful recovery of the sediment water interface.

According to the biogeochemical analysis in Gutiérrez et al. (2009) (i.e., palynofacies, oxygen index (Rock-Eval), total organic carbon and $\delta^{13}C$), B06 is characterized by a distinctive shift at ∼ 30 cm, more details are provided by Sifeddine et al. (2008) and Salvatteci et al. (2014a). The age model of B06 was inferred from five ^{14}C-calibrated accelerator mass spectrometry (AMS) age distributions (Fig. S1), showing that this core covers the last ∼ 700 years. For the last century, which is recorded only by B06, the age model was based on downcore natural excess ^{210}Pb and ^{137}Cs distributions and supported by bomb-derived ^{241}Am distributions (Fig. S2 and Gutiérrez et al., 2009). The mass accumulation rate after ca. AD 1950 was 0.036 ± 0.001 g cm^{-2} yr^{-1} and before ca. AD 1820 was 0.022 ± 0.001 g cm^{-2} yr^{-1}. On the other hand, G10 is a gravity-laminated sediment core of 5.22 m presenting six units and exhibiting some minor slumping. The G10 age model was based on 31 samples of ^{14}C-calibrated AMS age distributions, showing that the core covers the Holocene period (Salvatteci et al., 2014b, 2016). Here we used only a laminated section between ∼ 18 and 45 cm that chronologically covered part of the MCA period (from ∼ AD 1050 to 1500) and presented no slumps (Fig. S1).

The spatial regularity of the initial core sampling combined with the naturally variable sedimentation rate implied variable time rates between samples (150 samples in total). Each sample is 0.5 cm thick in B06 and usually includes 1–2 laminae. On the other hand, in core G10, each sample is 1 cm thick, including 3–4 laminae. The results considering the sedimentation rates showed that the intervals during MCA, LIA and CWP span 18, 7, and 3 years, respectively. Because of differences in the subsampling thickness between cores and variable sedimentation rates, results are binned by 20-year intervals (the lowest time resolution among samples) after linear interpolation and 20-year running mean of the original data set.

3.2 Grain size analyses

To isolate the mineral terrigenous fraction, organic matter, calcium carbonate and biogenic silica were successively removed from approximately 100 mg of bulk sediment sample using H_2O_2 (30 % at 50 °C for 3 to 4 days), HCl (10 % for 12 h) and Na_2CO_3 (1 M at 90 °C for 3 h), respectively. Between each chemical treatment, samples were repeatedly rinsed with deionized water and centrifuged at 4000 rpm until neutral pH. After pre-treatment, the grain size distribution was determined with an automated image analysis system (model FPIA3000, Malvern Instruments). This system is based on a CCD (charge-coupled device) camera that captures images of all of the particles homogeneously suspended in a dispersal solution by rotation (600 rpm) in a measurement cell. After magnification (×10), particle images are digitally processed and the equivalent spherical diameter (defined as the diameter of the spherical particle having the same surface as the measured particle) is determined. The optical magnification used (×10) allows the counting of particles with equivalent diameters between 0.5 and 200 µm. Prior to the FPIA analysis, all samples were sieved with a 200 µm mesh in order to recover coarser particles. Since particles > 200 µm were never found in any samples, the grain size distribution obtained by the FPIA method reliably represents the full particle size range in the sediment. A statistically significant number of particles (in the hundreds of thousands, up to 300 000) are automatically analyzed by FPIA, providing particle size information comparable to that obtained with a laser granulometer along with images of the individual particles. Using the images to check the efficiency of the pretreatments, we ensured that both organic matter and biogenic silica had been completely removed from all the samples. Finally, particle counts were binned into 45 different size bins between 0.5 and 200 µm instead of the 225 set by the FPIA manufacturer in order to reduce errors related to the presence of very few particles in some of the preselected narrow bins. Grain size distributions are expressed as (%) volume distributions.

3.3 Determining sedimentary components and the de-convolution fitting model

As different particle transport/deposition processes are known to influence the grain size distribution of the lithic fraction of sediment (e.g., Holz et al., 2007; Pichevin et al., 2005; Prins et al., 2007; Stuut et al., 2005, 2002; Sun et al., 2002; Weltje and Prins, 2003, 2007; Weltje, 1997), identifying the individual components of the polymodal grain size distribution is decisive for paleoenvironmental reconstructions. The numerical characteristics (i.e., amplitude (A), geometric mean diameter (Gmd), and geometric standard deviation (Gsd) of the individual grain size populations whose combination forms the overall grain size distribution) were determined for all samples using the iterative least-squares

method of Gomes et al. (1990). This fitting method aims to minimize the squared difference between the measured volume grain size distribution and the one computed from a mathematical expression based on lognormal function. The number of individual grain size populations to be used is determined by the operator, and all statistical parameters (A, Gmd and Gsd) are allowed to change from one sample to another. This process presents a strong advantage compared to end-member modeling (e.g., Weltje, 1997), in which the individual grain size distributions are maintained constant over the whole time series, the only fitting parameter being the relative amplitude, A. Indeed, it is unlikely that the parameters that govern both transport and deposition of lithogenic material, and therefore grain size of particles, remain constant over time. In turn, variations in these parameters are expected to induce changes in the grain size distribution parameters such as Gmd and Gsd.

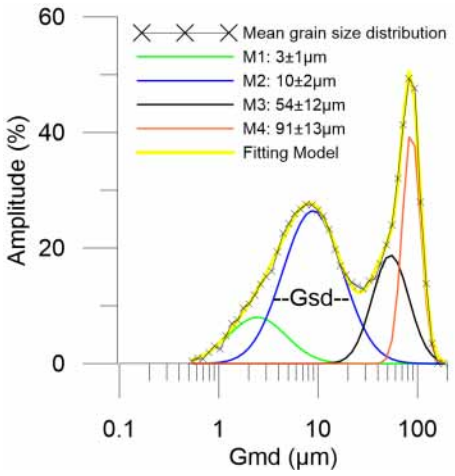

Figure 2. Comparison between a measured grain size distribution and the fitted curve using lognormal function and its partitioning into four individual grain size modes. The measured data are a mean grain size distribution from all samples of B6 and G10 cores.

4 Results and discussion

4.1 Basis for interpretation

Both sediment cores (B06 and G10) exhibit a roughly bimodal grain size distribution presenting significant variation in amplitude and width. These modes correspond to fine-grain-size classes from ~ 3 to 15 µm and coarser grain size classes between ~ 50 and 120 µm (Fig. S3). A principal component analysis (PCA) based on the Wentworth (1922) grain size classification identifies four modes that could explain the total variance of the data set (Fig. S4). The measured and computed grain size distributions show high correlations ranging from $R^2 = 0.75$ to 0.90, demonstrating that the use of four grain size modes is well adapted to our sediment samples and that the computed ones may be reliable for further interpretation (Fig. 2). Lower correlations only occurred for six samples that are characterized by small proportions of terrigenous material compared to biogenic silica, organic matter and carbonates. In these cases, the number of lithic particles remaining after chemical treatments was small, which increased the associated relative error. However, these samples have been included in the data set since they all presented a high contribution of coarser particles.

Grain size parameters are presented in Table 1. The first mode (M1), with a Gmd of approximately 3 ± 1 µm, and the second one (M2), with a Gmd of 10 ± 2 µm, are characterized by large Gsd ($\sim 2\sigma$), indicating a low degree of sorting. Such a low degree of sorting suggests a slow and continuous depositional process as occurs in other environments (Sun et al., 2002). The coarsest modes, M3 and M4, display mean Gmd values of 54 ± 12 and 91 ± 13 µm, respectively. These modes present Gsd values close to 1σ. The Gmd values of the two coarsest modes are consistent with the optimal grain size transported under conditions favorable to soil erosion (lack of vegetation, low threshold friction velocity, surface roughness and low soil moisture) and low wind friction velocity (Iversen and White, 1982; Kok et al., 2012; Marticorena and Bergametti, 1995; Marticorena, 2014; Shao and Lu, 2000). Such conditions prevail in the studied area because central coastal Peru consists of a sand desert area characterized by the absence of rain, a lack of vegetation and persistent wind (Gay, 2005; Haney and Grolier, 1991).

In the vicinity of desert areas, where wind-blown transport prevails, particles with grain size as high as ~ 100 µm can accumulate in marine sediments (e.g., Flores-Aqueveque et al., 2015; Stuut et al., 2007) or even in lacustrine sediments (An et al., 2012). Indeed, Stuut et al. (2007) reported the presence of distributions typical of wind-blown particles with ~ 80 µm grain size ($\sim 29°$ S North Chile), which is consistent with our results. In the studied area, the emission and transport of mineral particles are related to the strong wind events called *Paracas*. *Paracas* dust emission is a local seasonal phenomenon that preferentially occurs in winter (July–September) and is due to an intensification of the local surface winds (Escobar Baccaro, 1993; Haney and Grolier, 1991; Schweigger, 1984). The pressure gradient of sea level between 15 and 20° S, 75° W is the controlling factor of *Paracas* winds (Quijano, 2013), along with local topography (Gay, 2005). Coarse particles found in continental sediments off Pisco cannot have a fluvial origin because substantial hydrodynamic energy is necessary to mobilize particles of this size (50–100 µm), and this region is devoid of large rivers (Reinhardt et al., 2002; Scheidegger and Krissek, 1982; Suess et al., 1987).

Therefore, the coarsest modes (M3 and M4) can be interpreted as markers of aeolian transport resulting from surface winds and emission processes (Flores-Aqueveque et al., 2015; Hesse and McTainsh, 1999; Marticorena and Bergametti, 1995; McTainsh et al., 1997; Sun et al., 2002) and

Table 1. Averaged parameters (geometric mean diameter (Gmd), amplitude (A) and geometric standard deviation (Gsd)) of the four lognormal modes (components) identified from measured size distributions of sediment samples (B6 and G10 cores).

M1			M2			M3			M4		
Gmd (μm)	A (%)	Gsd	Gmd (μm)	A (%)	Gsd	Gmd (μm)	A (%)	Gsd	Gmd (μm)	A (%)	Gsd
3 ± 1	16 ± 7	1.9 ± 0.2	10 ± 2	43 ± 15	1.9 ± 0.2	54 ± 12	20 ± 10	1.4 ± 0.2	90 ± 13	20 ± 13	1.2 ± 0.2

indicate a local and proximal aeolian source (i.e., *Paracas* winds). This interpretation is in contrast to the Atacama Desert source suggested by Ehlert et al. (2015) and Molina-Cruz (1977). Ehlert et al. (2015), who used the same sediment core (B06), and also indicated difficulties in the interpretation of the detritical Sr isotopic signatures as an indicator of the terrigenous sources. These difficulties can be associated with the variability in the $^{87}Sr / ^{86}Sr$ due to grain size (Meyer et al., 2011). The finest M1 component (~ 3 μm) may be linked to both aeolian and fluvial transport mechanisms. Thus, because its origin is difficult to determine, and because its trend appears to be relatively independent of the other components, we do not use it further.

The M2 component (~ 10 μm) is interpreted as an indicator of fluvial transport (Koopmann, 1981; McCave et al., 1995; Stuut and Lamy, 2004; Stuut et al., 2002, 2007). Indeed, this is consistent with the report by Stuut et al. (2007) for the fluvial mud (~ 8 μm) in the south of Chile ($> 37°$ S), where the terrigenous input is dominated by fluvial origins. A fluvial origin of this M2 component is also supported by showing the same trend in the geochemical proxies, such as radiogenic isotope compositions of detrital components (Ehlert et al., 2015), mineral fluxes (Sifeddine et al., 2008) or %Ti (Salvatteci et al., 2014b), indicating more terrigenous transport during the LIA, when humid conditions were dominant. The M2 component is interpreted as being linked to river material discharge, mostly from the north Peruvian coast, and redistribution by the PCUC and bottom currents (Montes et al., 2010; Rein et al., 2004; Scheidegger and Krissek, 1982; Unkel et al., 2007).

4.2 Aeolian and fluvial input variability during the past ~1000 years

Grain size component (M2, M3 and M4; Table 1) variations in the composite records (B06 and G10) express changes in wind stress and fluvial runoff at multidecadal to centennial scales during the last millennium. The sediments deposited during the MCA exhibit two contrasting patterns of grain size distributions. A first sequence dated from AD 1050 to 1170 has low values of $D50$ (i.e., median grain size) that vary around 16 ± 6 μm and are explained by 50 ± 14 M2, 16 ± 8 M3, 21 ± 5 M4 and 13 ± 5 % M1 contributions. A second sequence, dated from AD 1170 to 1450, was marked by high values of $D50$ in the range of 34 ± 18 μm, with average contributions of 36 ± 8 for M2, 21 ± 10 for M3, 29 ± 15 for M4 and 14 ± 6 % for M1 (Table 2). These results indicate high variability in transport of particles during the MCA, with more fluvial sediment discharge from 1050 to 1170, followed by an aeolian transport increase between AD 1170 and 1450 (Fig. 3).

During the LIA (AD 1450–1800), the deposited particles were dominated by fine grain sizes with a $D50$ varying around an average of 15 μm, explained by 53 ± 15 % M2 contribution. In contrast, the contribution of M3 averaged 19 ± 9 % and ranged from 4 to 45 %, whereas M4 showed an average contribution of 14 ± 11 % and varied from 0 to 44 % during the same period. The dominant contribution of the finest-sized particles of M2 suggests a high fluvial terrigenous input to the Peruvian continental shelf. It is important to note that M2 contributions increased from the beginning to the end of the LIA at ~AD 1800, suggesting a gradual increase in fluvial sediment discharge input related to the enhancement of the continental precipitation (Fig. 3c). Indeed, during the LIA, our results confirm previous interpretations of wet conditions along the Peruvian coast (Gutiérrez et al., 2009; Salvatteci et al., 2014b; Sifeddine et al., 2008). These results also imply that this period was characterized by weak surface winds and hence a weaker coastal upwelling.

Subsequently, $D50$ variations show multidecadal variability during the last ~200 years that is divided into three distinctive periods. The first one, from ~AD 1800 to 1850, shows dominance of coarse particles around 50 μm, explained by the high contribution of M3 and M4 (up to 45 and 50 %, respectively) during this period. These results suggest a period of drier climate and very strong wind conditions. The second one, from AD 1850 to 1900, displays values around ~20 μm explained by ~40 of M2, ~20 of M3 and ~20 % of M4, suggesting that fluvial sediment discharge was the dominant transport mechanism, although not as significant as during the LIA. The third period spans from AD 1900 to the final part of record and covers the CWP. Our results reveal a dominance of coarse particles during the most of this period ($D50$ up to of 80 μm) that arise from high contributions of M3 and M4 (~40 and ~50 %, respectively). However, a clear decrease in the $D50$ is displayed at the end of this period that is explained by a decrease in contributions of the aeolian component M4 (~20 %), although the contribution of M3 and M2 remain relatively stable (~25 and 30 %, respectively). These conditions display no clear dominance of a given transport mode during this time. In addition, markedly coarser particles in the M4 component were very

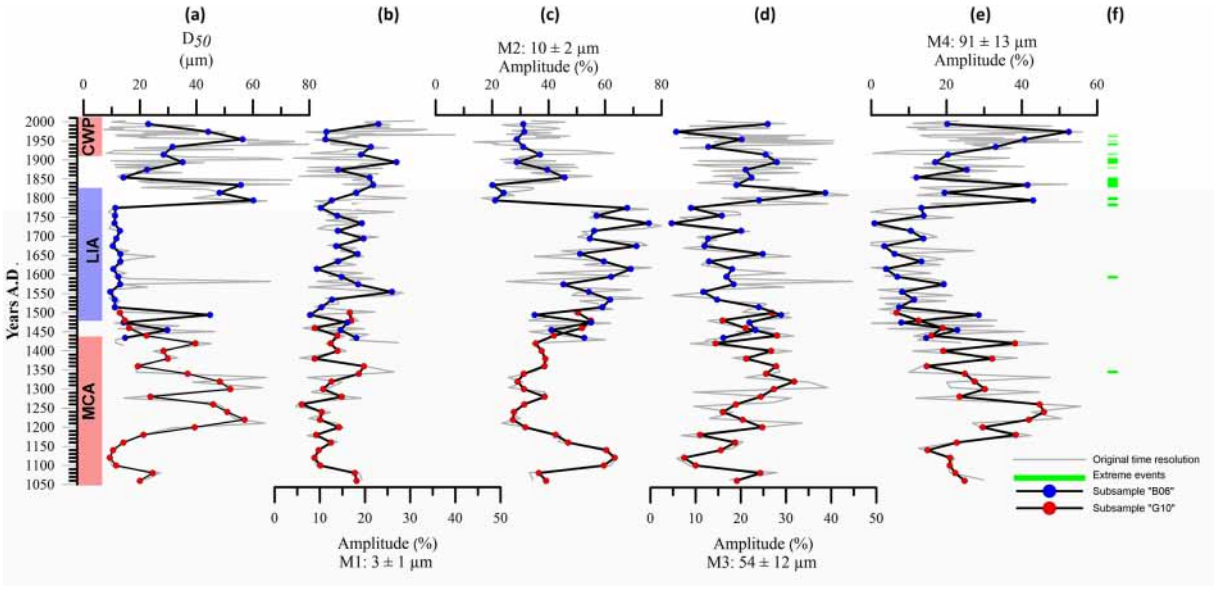

Figure 3. **(a)** Median grain size ($D50$) variation along the record and variation in relative abundance of the sedimentary components: **(b)** M1, **(c)** fluvial (M2), **(d)** aeolian (M3) and **(e)** aeolian (M4) of the grain size distribution in the record. **(f)** Samples where very large particles related to extreme events were found.

Table 2. Minimum, maximum and average values of the grain size components in each climate unit obtained along the record in the Pisco continental shelf.

	First period MCA AD 1050–1170		Second period MCA AD 1170–1450		LIA AD 1450–1800		CWP AD 1900 to present	
Grain size components	Amplitude (%)		Amplitude (%)		Amplitude (%)		Amplitude (%)	
	Av. ± SD	Range (min–max)	Av. ± SD	Range (min–max)	Av. ± SD	Range (min–max)	Av. ± SD	Range (min–max)
M1	13 ± 5	8–19	14 ± 6	5–27	15 ± 6	6–29	18 ± 7	4–40
M2	50 ± 14	33–64	36 ± 8	23–60	53 ± 15	16–80	34 ± 10	13–63
M3	16 ± 8	6–28	21 ± 10	0–39	19 ± 9	4–45	23 ± 10	6–44
M4	21 ± 5	12–30	29 ± 15	10–55	14 ± 11	0–44	25 ± 13	0–56

common during this time (the last 200 years), indicating a strong probability of extreme wind stress events (Fig. 3f).

4.3 Climatic interpretations

Our findings suggest a combination of regional and local atmospheric circulation mechanism changes that controlled the pattern of sedimentation in the study region. Our record is located under the contemporary seasonal *Paracas* dust storm path, but it also records discharged fluvial muds that are supplied by the rivers along the Peruvian coast. Hence, this record is particularly well suited for a reconstruction of continental runoff/wind intensity in the central Peruvian continental shelf during the last millennium. The interpretation of the changes in the single records of the components (M2, M3 and M4) and their associations (e.g., ratios) can reflect paleoclimatic variations in response to changes in atmospheric conditions. Here, we used the ratio between the aeolian components, defined as the contribution of the stronger winds over total wind variability: M4 / (M3 + M4). We consider this ratio to be a proxy of the local wind surface intensity and thus of the SPSH atmospheric circulation (Fig. 4a). Previous studies have similarly and successfully used grain size fraction ratios as paleoclimate proxies of atmospheric conditions and circulation to explain other sediment records (Holz et al., 2007; Huang et al., 2011; Prins, 1999; Shao et al., 2011; Stuut et al., 2002; Sun et al., 2002; Weltje and Prins, 2003).

As explained above, the MCA was characterized by a sine-like peak structure that depicts two different climate stages. During the first stage, spanning from ∼ AD 1050 to 1170, the fluvial input show a peak centered at AD 1120 that was linked to a precipitation increase accompanied by a decrease

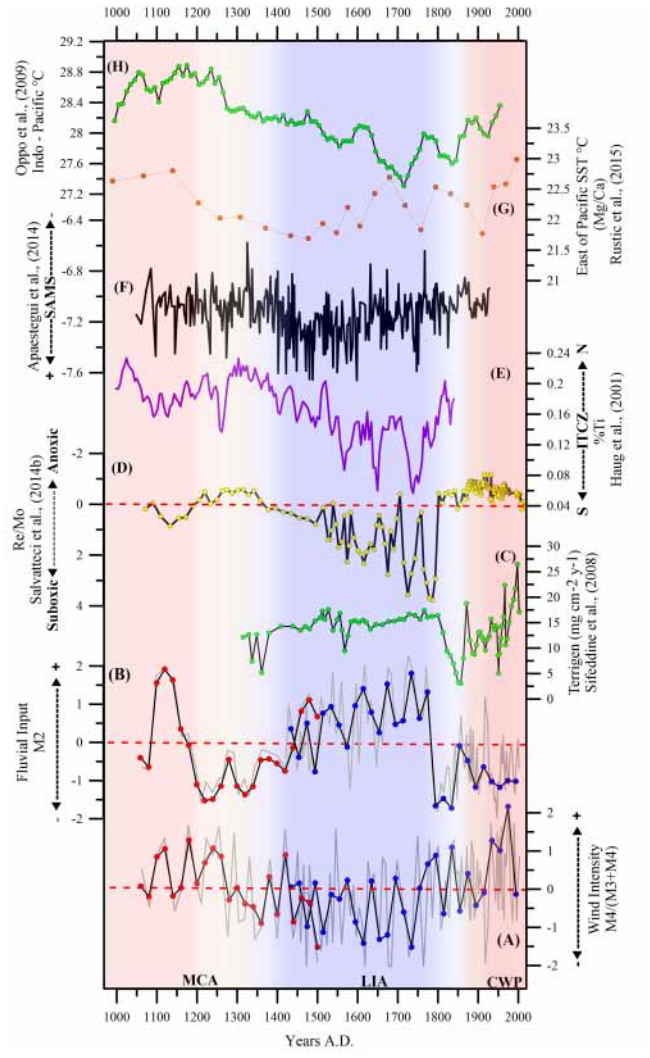

Figure 4. **(a)** Wind intensity (M4 / (M3 + M4)) anomaly reconstruction, **(b)** fluvial input (M2) anomaly reconstruction on the continental shelf, and records of **(c)** terrigenous flux (total minerals) in Pisco continental shelf by Sifeddine et al. (2008), **(d)** OMZ activity (Re / Mo anomalies) negative values indicate more anoxic conditions (the axis was reversed) (Salvatteci et al., 2014b), **(e)** ITCZ migration (%Ti) (Peterson and Haug, 2006), **(f)** SAMS activity reconstruction (δ^{18}O Palestina Cave) (Apaéstegui et al., 2014), **(g)** eastern temperatures reconstruction (Rustic et al., 2015) and **(h)** Indo-Pacific temperatures reconstruction (Oppo et al., 2009).

in wind intensity. Those results suggest a southward ITCZ displacement (Fig. 4e) as a response to more El Niño-like conditions as suggested by Rustic et al. (2015) (Fig. 4g and h). In contrast, during the second stage the surface winds had their greatest intensity with a peak centered at ∼ AD 1200 as a consequence of displacement of the ITCZ–SPSH system. The displacement of the SPSH core towards the eastern South American coast intensified alongshore winds as a regional response to stronger Walker circulation. These features are in agreement with the ocean thermostat mechanism proposed by Clement et al. (1996). This mechanism produces a shallow thermocline in the eastern Pacific (Fig. 4g and h) and consequently more intense upwelling conditions and a stronger OMZ offshore of Pisco recorded in low values of the Re / Mo ratio (Fig. 4d). These two patterns (i.e., enhanced fluvial transport/enhanced wind intensity) might have been triggered by the expression of Pacific variability at multidecadal timescales with the combined action of the Atlantic Multidecadal Oscillation (AMO). Indeed, other works provide evidence during the MCA for low South American monsoon system (SAMS) activity at multidecadal timescales driven by the AMO (Fig. 4f) (Apaéstegui et al., 2014; Bird et al., 2011; Reuter et al., 2009). Thus, besides the displacement of the ITCZ, the AMO could have modulated Walker circulation at a multidecadal variability during the MCA through mechanisms such as those described by McGregor et al. (2014) and Timmermann et al. (2007).

Our results, combined with other paleo-reconstructions, suggest that the LIA was accompanied by a weakening of the regional atmospheric circulation and of the upwelling favorable winds. During the LIA, the mean climate state was controlled by a gradual intensification of the fluvial input of sediments to the continental shelf, thus indicating more El Niño-like conditions (Fig. 4b). These features are confirmed by an increase in the terrigenous sediment flux, as described by Sifeddine et al. (2008) (Fig. 4c) and Gutiérrez et al. (2009) and by changes of the radiogenic isotopic composition of the terrigenous fraction (Ehlert et al., 2015). These wet conditions are also marked by an intensification of the SAMS and the southern meridional displacement of the ITCZ, as evidenced by paleo-precipitation records in the Andes and in the Cariaco Trench (Apaéstegui et al., 2014; Haug et al., 2001; Peterson and Haug, 2006) (Fig. 4e). At the same time, a prevalence of weak surface winds (Fig. 4a) and an increase in subsurface oxygenation driving sub-oxic conditions in the surface sediment are recorded (Fig. 4d). These characteristics also support the hypothesis of the ITCZ–SPSH southern meridional displacement and are consistent with a weakening of the Walker circulation (Fig. 4g).

The transition period between the LIA and CWP appears as an abrupt event showing a progressive positive anomaly in the wind intensity synchronous with a rapid decrease in fluvial input to the continental shelf (Fig. 4a and b). This transition suggests a rapid change of meridional (ITCZ–SPSH) and zonal (Walker) circulation interconnection, which controls the input of terrigenous material (fluvial/aeolian). Gutiérrez et al. (2009) found evidence of a large reorganization in the tropical Pacific climate with immediate effects on ocean biogeochemical cycling and ecosystem structure at the transition between the LIA and CWP. The increase in the regional wind circulation that favors aeolian erosive processes simultaneously leads to an increase in the OMZ intensity related to upwelling intensification.

Finally, during the CWP (∼ AD 1900 to present), a trend to steadying of low fluvial input (Fig. 4b) was combined with

an increase in wind intensity (Fig. 4a) that was coupled to a strong OMZ. This setting suggests the northernmost ITCZ–SPSH system position. This hypothesis is supported by other studies on the continental shelf of Peru (Salvatteci et al., 2014b) and also in the eastern Andes, where a decrease in rainfall of between ∼ 10 and 20 % relative to the LIA was reported for the last century (Reuter et al., 2009). Enhancement of wind intensity is also consistent with the multidecadal coastal cooling and increase in upwelling productivity since the late nineteenth century (Gutiérrez et al., 2011; Salvatteci et al., 2014b; Sifeddine et al., 2008) and confirms the relations between the intensification of the upwelling activity induced by the variability in the regional wind intensity from SPSH displacement.

The increase in the wind intensity over the past two centuries likely represents a result of the modern positioning of the ITCZ–SPSH system and the associated intensification of the local and regional winds (Fig. 4a). The contributions of aeolian deposition material (Fig. 3e and f) and, as a consequence, the wind intensity and its variability during the last 100 years are stronger than during the second sequence of the MCA (Fig. 4a) under similar conditions (i.e., position of the ITCZ–SPSH system). This variability implies a forcing mechanism in addition to the enhancement of the wind intensity, one that may be related to the current climate change conditions (Bakun, 1990; England et al., 2014; Sydeman et al., 2014). Moreover, during the CWP, the wind intensity showed a direct relation with OMZ strength (Fig. 4a and d) that suggests an increase in the zonal gradient and thus in the Walker circulation on a multidecadal scale.

Our record shows that on a centennial scale, the fluvial input changes are driven by the meridional ITCZ position and a weak gradient of the Walker circulation, consistent with El Niño-like conditions. In contrast, variations in the surface wind intensity are linked to the position of the SPSH modulated by both the meridional variation in the ITCZ and the intensification of the zonal gradient temperature related to the Walker circulation and expressing La Niña-like conditions. A clear relation between the zonal circulation and wind intensity at a centennial timescale is displayed. All these features modulate the biogeochemical behavior of the Peruvian upwelling system.

5 Conclusions

Study of the grain size distribution in laminated sediments from the Pisco Peruvian shelf has allowed the reconstruction of changes in wind intensity and terrigenous fluvial input at centennial and multidecadal timescales during the last millennium. The long-term variation in the M2 (∼ 10 µm) mode is an indicator of hemipelagic fluvial input related to the regional precipitation variability. At the same time, the M3 (54 ± 11 µm) and M4 (91 ± 11 µm) components are related to aeolian transport and thus with both local and regional wind intensity. The temporal variations in these fractions indicate that the MCA and CWP periods were characterized by an increment in the coarse-particle transport (M3 and M4) and thus an enhancement of the surface wind intensity, whereas the LIA was characterized by stronger fluvial input as evidenced from an increase in fine (M2) particles. Comparison between records reveals a coherent match between the meridional displacement of the ITCZ–SPSH system and the regional fluvial and aeolian terrigenous input variability. The ITCZ–SPSH system northern displacement during the second period of the MCA and the CWP was associated with the intensification of the Walker cell and La Niña Like conditions, resulting in stronger winds, upwelling-favorable conditions, enhanced marine productivity and greater oxygen depletion in the water column. In contrast, the southward migrations of the ITCZ–SPSH system during the LIA correspond to an enhancement to the South American monsoon circulation and El Niño-like conditions, driving the increase in the precipitation and the terrigenous fluvial input to the Pisco continental shelf, lower productivity and increased oxygenation. Two patterns observed during the MCA, respectively marked by fluvial intensification and wind intensification, could have been forced by Pacific Ocean variability at multidecadal timescales. Further studies of the paleowind reconstruction at high time resolution, combined with model simulation, are needed to better understand the interplay between the Pacific and Atlantic Ocean connection on climate variability as evidenced by McGregor et al. (2014) in the modern Pacific climate pattern.

The Supplement related to this article is available online at doi:10.5194/cp-12-787-2016-supplement.

Acknowledgements. This work was supported by the International Joint Laboratory "PALEOTRACES" (IRD, France; UPMC, France; UFF, Brazil; UA, Chile; UPCH, Peru), the Department of Geochemistry of the Universidade Federal Fluminense (UFF, Brazil), the ALYSES analytical platform (IRD/UPMC, supported by grants from Région Ile-de-France), the Peruvian Marine Research Institute (IMARPE) and the Geophysical Institute of Peru (IGP). It was also supported by the collaborative project Chaire Croisée PROSUR (IRD). We are deeply grateful to CAPES (Brazil) for the scholarship to Francisco Briceño Zuluaga. We give special thanks to Ioanna Bouloubassi and Phil Meyers for their comments and suggestions. We are also grateful to the anonymous reviewers for their constructive and helpful suggestions, which helped to improve this manuscript.

Edited by: J. Martinez

References

An, F., Ma, H., Wei, H., and Lai, Z.: Distinguishing aeolian signature from lacustrine sediments of the Qaidam Basin in northeastern Qinghai-Tibetan Plateau and its palaeoclimatic implications, Aeolian Res., 4, 17–30, 2012.

Apaéstegui, J., Cruz, F. W., Sifeddine, A., Vuille, M., Espinoza, J. C., Guyot, J. L., Khodri, M., Strikis, N., and Perú, G.: Hydroclimate variability of the northwestern Amazon Basin near the Andean foothills of Peru related to the South American Monsoon System during the last 1600 years, Clim. Past, 10, 1967–1981, doi:10.5194/cp-10-1967-2014, 2014.

Bakun, A.: Global climate change and intensification of coastal ocean upwelling, Science, 247, 198–201, 1990.

Bekaddour, T., Schlunegger, F., Vogel, H., Delunel, R., Norton, K. P., Akçar, N., and Kubik, P.: Paleo erosion rates and climate shifts recorded by Quaternary cut-and-fill sequences in the Pisco valley, central Peru, Earth Planet. Sc. Lett., 390, 103–115, 2014.

Bendix, A., Bendix, J., Gämmerler, S., Reudenbach, C., and Weise, S.: The El Niño 1997/98 as seen from space – rainfall retrieval and investigation of rainfall dynamics with Goes-8 and TRMM Data, in The 2002 EUMETSAT Meteor. Satellite Conf., Dublin, Ireland 2–6 September 2002, EUM P, 36, 647–652, 2002.

Bird, B. W., Abbott, M. B., Vuille, M., Rodbell, D. T., Stansell, N. D., and Rosenmeier, M. F.: A 2,300-year-long annually resolved record of the South American summer monsoon from the Peruvian Andes, P. Natl. Acad. Sci. USA, 108, 8583–8, 2011.

Bloemsma, M. R., Zabel, M., Stuut, J. B. W., Tjallingii, R., Collins, J. A., and Weltje, G. J.: Modelling the joint variability of grain size and chemical composition in sediments, Sediment. Geol., 280, 135–148, 2012.

Böning, P. and Brumsack, H.: Geochemistry of Peruvian near-surface sediments, Geochim. Cosmochim. Acta, 68, 4429–4451, 2004.

Brodie, I. and Kemp, A. E. S.: Variation in Biogenic and Detrital Fluxes and Formation of Laminae in Late Quaternary Sediments from the Peruvian Coastal Upwelling Zone, Mar. Geol., 116, 385–398, 1994.

Chaigneau, A., Dominguez, N., Eldin, G., Vasquez, L., Flores, R., Grados, C., and Echevin, V.: Near-coastal circulation in the Northern Humboldt Current System from shipboard ADCP data, J. Geophys. Res.-Ocean., 118, 5251–5266, 2013.

Clement, A. C., Seager, R., Cane, M. A., and Zebiak, S. E.: An ocean dynamical thermostat, J. Climate, 9, 2190–2196, 1996.

Ehlert, C., Grasse, P., Gutiérrez, D., Salvatteci, R., and Frank, M.: Nutrient utilisation and weathering inputs in the Peruvian upwelling region since the Little Ice Age, Clim. Past, 11, 187–202, doi:10.5194/cpd-10-3357-2014, 2015.

England, M. H., McGregor, S., Spence, P., Meehl, G. A., Timmermann, A., Cai, W., Gupta, A. Sen, McPhaden, M. J., Purich, A., and Santoso, A.: Recent intensification of wind-driven circulation in the Pacific and the ongoing warming hiatus, Nature Climatic Change, 4, 222–227, 2014.

Escobar Baccaro, D. F.: Evaluacion climatologica y sinoptica del fenómeno de vientos Paracas, Universidad Nacional Agraria La Molina, Lima-Peru, 1993.

Flores-Aqueveque, V., Alfaro, S. C., Caquineau, S., Foret, G., Vargas, G., and Rutllant, J. A.: Inter-annual variability of southerly winds in a coastal area of the Atacama Desert: implications for the export of aeolian sediments to the adjacent marine environment, Sedimentology, 59, 990–1000, 2012.

Flores-Aqueveque, V., Alfaro, S., Vargas, G., Rutllant, J. A., and Caquineau, S.: Aeolian particles in marine cores as a tool for quantitative high-resolution reconstruction of upwelling favorable winds along coastal Atacama Desert, Northern Chile, Prog. Oceanogr., 134, 244–255, 2015.

Garreaud, R. D. and Falvey, M.: The coastal winds off western subtropical South America in future climate scenarios, Int. J. Climatol., 29, 543–554, 2009.

Gay, S. P.: Blowing sand and surface winds in the Pisco to Chala Area, Southern Peru, J. Arid Environ., 61, 101–117, 2005.

Gomes, L., Bergametti, G., Dulac, F., and Ezat, U.: Assessing the actual size distribution of atmospheric aerosols collected with a cascade impactor, J. Aerosol Sci., 21, 47–59, 1990.

Gutiérrez, D., Sifeddine, A., Reyss, J., Vargas, G., Velasco, F., Salvatteci, R., Ferreira, V., Ortlieb, L., Field, D., Baumgartner, T., Boussafir, M., Boucher, H., Valdes, J., Marinovic, L., Soler, P., and Tapia, P.: Anoxic sediments off Central Peru record interannual to multidecadal changes of climate and upwelling ecosystem during the last two centuries, Adv. Geosci., 6, 119–125, 2006.

Gutiérrez, D., Sifeddine, A., Field, D. B., Ortlieb, L., Vargas, G., Chávez, F. P., Velazco, F., Ferreira, V., Tapia, P., Salvatteci, R., Boucher, H., Morales, M. C., Valdés, J., Reyss, J.-L., Campusano, A., Boussafir, M., Mandeng-Yogo, M., García, M., and Baumgartner, T.: Rapid reorganization in ocean biogeochemistry off Peru towards the end of the Little Ice Age, Biogeosciences, 6, 835–848, doi:10.5194/bg-6-835-2009, 2009.

Gutiérrez, D., Bouloubassi, I., Sifeddine, A., Purca, S., Goubanova, K., Graco, M., Field, D., Méjanelle, L., Velazco, F., Lorre, A., Salvatteci, R., Quispe, D., Vargas, G., Dewitte, B., and Ortlieb, L.: Coastal cooling and increased productivity in the main upwelling zone off Peru since the mid-twentieth century, Geophys. Res. Lett., 38, 1–6, 2011.

Haney, E. M. and Grolier, M. J.: Geologic map of major Quaternary eolian features, northern and central coastal Peru, United States Geol. Surv. Misc. Investig., I-2162, 1991.

Haug, G. H., Hughen, K. A., Sigman, D. M., Peterson, L. C., and Röhl, U.: Southward migration of the intertropical convergence zone through the Holocene, Science, 293, 1304–8, 2001.

Hesse, P. P. and McTainsh, G. H.: Last Glacial Maximum to Early Holocene Wind Strength in the Mid-latitudes of the Southern Hemisphere from Aeolian Dust in the Tasman Sea, Quaternary Res., 52, 343–349, 1999.

Hill, E. A., Hickey, B. M., Shillington, F. A., Strub, P. T., Brink, K. H., Barton, E. D., and Thomas, A. C.: Eastern Ocean Boundaries coastal segment (E), in: The Sea, Vol 11, edited by: Robinson, A. and Brink, K., John Wiley & Sons Ltd., 29–67, 1998.

Holz, C., Stuut, J. B. W., Henrich, R., and Meggers, H.: Variability in terrigenous sedimentation processes off northwest Africa and its relation to climate changes: Inferences from grain-size distributions of a Holocene marine sediment record, Sediment. Geol., 202, 499–508, 2007.

Huang, X., Oberhänsli, H., von Suchodoletz, H., and Sorrel, P.: Dust deposition in the Aral Sea: implications for changes in atmospheric circulation in central Asia during the past 2000 years, Quaternary Sci. Rev., 30, 3661–3674, 2011.

Iversen, J. D. and White, B. R.: Saltation threshold on Earth, Mars and Venus, Sedimentology, 29, 111–119, 1982.

Kok, J. F., Parteli, E. J. R., Michaels, T. I., and Karam, D. B.: The physics of wind-blown sand and dust, Reports Prog. Phys., 75, 106901, doi:10.1088/0034-4885/75/10/106901, 2012.

Koopmann, B.: Sedimentation von Saharastaub im subtropischen Nordatlantik während der letzten 25.000 Jahre, Meteor Forsch. Ergeb. R. C, 35, 23–59, 1981.

Lavado-Casimiro, W. and Espinoza, J. C.: Impacts of El Nino and La Nina in the precipitation over Peru (1965–2007), Rev. Bras. Meteorol., 29, 171–182, 2014.

Lavado Casimiro, W., Ronchail, J., Labat, D., Espinoza, J. C., and Guyot, J. L.: Basin-scale analysis of rainfall and runoff in Peru (1969–2004): Pacific, Titicaca and Amazonas drainages, Hydrol. Sci. J., 57, 625–642, 2012.

Marticorena, B.: Dust Production Mechanisms, in: Mineral Dust: A Key Player in the Earth System, edited by: Knippertz, P. and Stuut, J.-B., Springer, Dordrecht Heidelberg New York London, 93–120, 2014.

Marticorena, B. and Bergametti, G.: Modeling the atmospheric dust cycle: 1. Design of a soil-derived dust emission scheme, J. Geophys. Res., 100, 16415, doi:10.1029/95JD00690, 1995.

McCave, I. N., Manighetti, B., and Robinson, S. G.: Sortable silt and fine sediment size/composition slicing: parameters for palaeocurrent speed and Palaeoceanography, Palaeoceanography, 10, 593–610, 1995.

McGregor, S., Timmermann, A., Stuecker, M. F., England, M. H., and Merrifield, M.: Recent Walker circulation strengthening and Pacific cooling amplified by Atlantic warming, Nature Climatic Change, 4, 1–5, 2014.

McPhillips, D., Bierman, P. R., Crocker, T., and Rood, D. H.: Landscape response to Pleistocene-Holocene precipitation change in the Western Cordillera, Peru: 10 Be concentrations in modern sediments and terrace fills, J. Geophys. Res. Earth Surf., 118, 2488–2499, 2013.

McTainsh, G. H., Nickling, W. G., and Lynch, A. W.: Dust deposition and particle size in Mali, West Africa, Catena, 29, 307–322, 1997.

Meyer, I., Davies, G. R., and Stuut, J. B. W.: Grain size control on Sr-Nd isotope provenance studies and impact on paleoclimate reconstructions: An example from deep-sea sediments offshore NW Africa, Geochem. Geophyst. Geosys., 12, 14, 3, doi:10.1029/2010GC003355, 2011.

Molina-Cruz, A.: The relation of the southern trade winds to upwelling processes during the last 75,000 years, Quaternary Res., 8, 324–338, 1977.

Montes, I., Colas, F., Capet, X., and Schneider, W.: On the pathways of the equatorial subsurface currents in the eastern equatorial Pacific and their contributions to the Peru-Chile Undercurrent, J. Geophys. Res.-Ocans, 115, 1–16, 2010.

Morera, S., Condom, T., Crave, A., and Galvez, C.: Tasas de erosión y dinámica de los flujos de sedimentos en la cuenca del río Santa, Perú, Rev. Peru. Geo-Atmosférica, 37, 25–37, 2011.

Oppo, D. W., Rosenthal, Y., and Linsley, B. K.: 2,000-year-long temperature and hydrology reconstructions from the Indo-Pacific warm pool, Nature, 460, 1113–1116, 2009.

Ortlieb, L.: The Documented Historical Record of El Nino Events in Peru: An Update of the Quinn Record (Sixteenth throught Nineteenth Centuries), in: El Nino and the Southern Oscillation, Multiscale Variability and Global and Regional Impacts, 207–295, 2000.

Parkin, D. W. and Shackleton, N.: Trade wind and temperature correlations down a deep sea core off the Sharan coast, Nature, 245, 455–457, 1973.

Peterson, L. and Haug, G.: Variability in the mean latitude of the Atlantic Intertropical Convergence Zone as recorded by riverine input of sediments to the Cariaco Basin (Venezuela), Palaeogeogr. Paleoceanogr., 234, 97–113, 2006.

Pichevin, L., Cremer, M., Giraudeau, J., and Bertrand, P.: A 190 ky record of lithogenic grain-size on the Namibian slope: Forging a tight link between past wind-strength and coastal upwelling dynamics, Mar. Geol., 218, 81–96, 2005.

Prins, M.: Pelagic, hemipelagic and turbidite deposition in the Arabian Sea during the late Quaternary: Unravelling the signals of aeolian and fluvial sediment supply as functions of tectonics, sea-level and climate change by means of end-member modelling of silicic, Utrecht, Universiteit Utrecht, 1999.

Prins, M. A., Vriend, M., Nugteren, G., Vandenberghe, J., Lu, H., Zheng, H., and Jan Weltje, G.: Late Quaternary aeolian dust input variability on the Chinese Loess Plateau: inferences from unmixing of loess grain-size records, Quaternary Sci. Rev., 26, 230–242, 2007.

Quijano Vargas, J. J.: Estudio numerico y observacional de la dinámica de Viento Paracas, asociado al transporte eólico hacia el océano frente a la costa de Ica-Perú, Universidad Peruana Cayetano Heredia, Lima, Perú, 2013.

Ratmeyer, V., Fischer, G., and Wefer, G.: Lithogenic particle fluxes and grain size distributions in the deep ocean off northwest Africa: Implications for seasonal changes of aeolian dust input and downward transport, Deep-Sea Res. Pt. I, 46, 1289–1337, 1999.

Rein, B.: El Niño variability off Peru during the last 20,000 years, Paleoceanography, 20, PA4003, doi:10.1029/2004PA001099, 2005.

Rein, B.: How do the 1982/83 and 1997/98 El Niños rank in a geological record from Peru?, Quaternary Int., 161, 56–66, 2007.

Rein, B., Lückge, A., and Sirocko, F.: A major Holocene ENSO anomaly during the Medieval period, Geophys. Res. Lett., 31, L17211, doi:10.1029/2004GL020161, 2004.

Reinhardt, L., Kudrass, H., Lückge, A., Wiedicke, M., Wunderlich, J., and Wendt, G.: High-resolution sediment echosounding off Peru Late Quaternary depositional sequences and sedimentary structures of a current-dominated shelf, Mar. Geophys. Res., 23, 335–351, 2002.

Reuter, J., Stott, L., Khider, D., Sinha, A., Cheng, H., and Edwards, R. L.: A new perspective on the hydroclimate variability in northern South America during the Little Ice Age, Geophys. Res. Lett., 36, L21706, doi:10.1029/2009GL041051, 2009.

Rustic, G. T., Marchitto, T. M., and Linsley, B. K.: Dynamical excitation of the tropical Pacific Ocean and ENSO variability by Little Ice Age cooling, Science, 350, 1537–1541, 2015.

Salvatteci, R., Field, D. B., Baumgartner, T., Ferreira, V., and Gutierrez, D.: Evaluating fish scale preservation in sediment records from the oxygen minimum zone off Peru, Paleobiology, 38, 52–78, 2012.

Salvatteci, R., Field, D., Sifeddine, A., Ortlieb, L., Ferreira, V., Baumgartner, T., Caquineau, S., Velazco, F., Reyss, J. L., Sanchez-Cabeza, J. A., and Gutierrez, D.: Cross-stratigraphies

from a seismically active mud lens off Peru indicate horizontal extensions of laminae, missing sequences, and a need for multiple cores for high resolution records, Mar. Geol., 357, 72–89, 2014a.

Salvatteci, R., Gutierrez, D., Field, D., Sifeddine, A., Ortlieb, L., Bouloubassi, I., Boussafir, M., Boucher, H., and Cetin, F.: The response of the Peruvian Upwelling Ecosystem to centennial-scale global change during the last two millennia, Clim. Past, 10, 1–17, doi:10.5194/cp-10-1-2014, 2014b.

Salvatteci, R., Gutierrez, D., Sifeddine, A., Ortlieb, L., Druffel, E., Boussafir, M., and Schneider, R.: Centennial to millennial-scale changes in oxygenation and productivity in the Eastern Tropical South Pacific during the last 25,000 years, Quaternary Sci. Rev., 131, 102–117, 2016.

Saukel, C., Lamy, F., Stuut, J. B. W., Tiedemann, R., and Vogt, C.: Distribution and provenance of wind-blown SE Pacific surface sediments, Mar. Geol., 280, 130–142, 2011.

Scheidegger, K. F. and Krissek, L. A.: Dispersal and deposition of eolian and fluvial sediments off Peru and northern Chile, Geol. Soc. Am. Bull., 93, 150–162, 1982.

Schweigger, E.: El litoral peruano (Segunda edicioìn), Lima, Universidad Nacional "Federico Villarreal", 1964, 1984.

Sears, M.: Notes on the Peruvian coastal current, 1. An introduction to the ecology of Pisco Bay, Deep-Sea Res., 1, 141–169, 1954.

Shao, Y. and Lu, H.: A simple expression for wind erosion threshold friction velocity, J. Geophys. Res., 105, 22437, doi:10.1029/2000JD900304, 2000.

Shao, Y., Ishizuka, M., Mikami, M., and Leys, J. F.: Parameterization of size-resolved dust emission and validation with measurements, J. Geophys. Res.-Atmos., 116, 1–19, 2011.

Sifeddine, A., Gutiérrez, D., Ortlieb, L., Boucher, H., Velazco, F., Field, D., Vargas, G., Boussafir, M., Salvatteci, R., Ferreira, V., García, M., Valdés, J., Caquineau, S., Mandeng Yogo, M., Cetin, F., Solis, J., Soler, P., and Baumgartner, T.: Laminated sediments from the central Peruvian continental slope: A 500 year record of upwelling system productivity, terrestrial runoff and redox conditions, Prog. Oceanogr., 79, 190–197, 2008.

Smith, R. L.: Circulation patterns in upwelling regimes, Coast. upwelling, 13–35, 1983.

Strub, P. T., Mesías, J. M. J. M., Montecino, V., Rutllant, J. A., Salinas, S., Robinson, A. R., and Brink, K. H.: Coastal ocean circulation off western South America, The Sea, 11, 273–313., 1998.

Stuut, J.-B. W. and Lamy, F.: Climate variability at the southern boundaries of the Namib (southwestern Africa) and Atacama (northern Chile) coastal deserts during the last 120,000 yr, Quaternary Res., 62, 301–309, 2004.

Stuut, J.-B. W., Prins, M. a., Schneider, R. R., Weltje, G. J., Jansen, J. H. F., and Postma, G.: A 300-kyr record of aridity and wind strength in southwestern Africa: inferences from grain-size distributions of sediments on Walvis Ridge, SE Atlantic, Mar. Geol., 180, 221–233, 2002.

Stuut, J.-B. W., Prins, M. A., and Weltje, G. J.: The palaeoclimatic record provided by aeolian dust in the deep sea: proxies and problems, Geophys. Res. Abstr., 7, 10886, doi:10.1607-7962/gra/EGU05-A-10886, 2005.

Stuut, J.-B. W., Kasten, S., Lamy, F., and Hebbeln, D.: Sources and modes of terrigenous sediment input to the Chilean continental slope, Quaternary Int., 161, 67–76, 2007.

Suess, E., Kulm, L. D., and Killingley, J. S.: Coastal upwelling and a history of organic-rich mudstone deposition off Peru, Geol. Soc. London, 26, 181–197, 1987.

Sun, D., Bloemendal, J., Rea, D., Vandenberghe, J., Jiang, F., An, Z., and Su, R.: Grain-size distribution function of polymodal sediments in hydraulic and aeolian environments, and numerical partitioning of the sedimentary components, Sediment. Geol., 152, 263–277, 2002.

Sydeman, W. J., García-Reyes, M., Schoeman, D. S., Rykaczewski, R. R., Thompson, S. A., Black, B. A., and Bograd, S. J.: Climate change and wind intensification in coastal upwelling ecosystems, Science, 345, 77–80, 2014.

Timmermann, A., Okumura, Y., An, S. I., Clement, A., Dong, B., Guilyardi, E., Hu, A., Jungclaus, J. H., Renold, M., Stocker, T. F., Stouffer, R. J., Sutton, R., Xie, S. P., and Yin, J.: The influence of a weakening of the Atlantic meridional overturning circulation on ENSO, J. Climate, 20, 4899–4919, 2007.

Unkel, I., Kadereit, A., Mächtle, B., Eitel, B., Kromer, B., Wagner, G., and Wacker, L.: Dating methods and geomorphic evidence of palaeoenvironmental changes at the eastern margin of the South Peruvian coastal desert (14°30′ S) before and during the Little Ice Age, Quaternary Int., 175, 3–28, 2007.

Weltje, G. J.: End-member modeling of compositional data: Numerical-statistical algorithms for solving the explicit mixing problem, Math. Geol., 29, 503–549, 1997.

Weltje, G. J. and Prins, M. A.: Muddled or mixed? Inferring palaeoclimate from size distributions of deep-sea clastics, Sediment. Geol., 162, 39–62, 2003.

Weltje, G. J. and Prins, M. A.: Genetically meaningful decomposition of grain-size distributions, Sediment. Geol., 202, 409–424, 2007.

Wentworth, C. K.: A Scale of Grade and Class Terms for Clastic Sediments, J. Geol., 30, 377–392, 1922.